# Wave-Field Formation in a Hollow X-Ray Waveguide

I. Bukreeva,[1,2] A. Popov,[3] D. Pelliccia,[1,4] A. Cedola,[1] S. B. Dabagov,[2,5] and S. Lagomarsino[1]

[1]*Istituto Fotonica e Nanotecnologie (IFN), Consiglio Nazionale delle Ricerche, Via Cineto Romano 42, 00156 Roma, Italy*
[2]*Russian Academy of Science, P. N. Lebedev Physics Institute, Leninsky pr. 53, 119991 Moscow, Russia*
[3]*Institute of Terrestrial Magnetism, Ionosphere and Radiowave Propagation, Troitsk, Moscow region, 142092, Russia*
[4]*Dipartimento Fisica, Università "La Sapienza" and Istituto Nazionale di Fisica Nucleare, Sezione Roma1, Rome, Italy*
[5]*Istituto Nazionale di Fisica Nucleare (INFN), Laboratori Nazionali di Frascati, Via E. Fermi, 40, 00044 Frascati (RM), Italy*

(Received 5 July 2006; published 30 October 2006)

Diffraction and refraction phenomena at the entrance of a hollow x-ray waveguide with weakly absorbing dielectric cladding layers are investigated using two independent approaches: (a) analytical and (b) numerical solutions of the wave equation in the paraxial (parabolic) approximation. It is shown that the wave penetrating through the cladding material substantially modifies the wave field near the waveguide entrance. It results in a significant increase of the total energy flux inside the guiding layer and in additional spatial modulation of the electromagnetic field.

DOI: 10.1103/PhysRevLett.97.184801 PACS numbers: 41.50.+h, 42.82.Et, 61.10.−i

The advancement of nanoscience and nanotechnology in many fields requires the development of proper tools with nanometer spatial resolution. X rays have many peculiarities which make them suitable for studies of nano-objects: short wavelength, penetrating power, capability to probe samples in their natural environment, etc. This is the reason why considerable effort is currently devoted to the development of x-ray optical elements capable of providing x-ray beams with the required size, divergence, and coherence properties.

X-ray waveguides (WGs), proposed for the first time in 1974 by Spiller and Segmüller [1], are intensively studied because they can provide fully coherent beams as small as 10 nm [2,3] in the hard x-ray region. X-ray microdiffraction with a record spatial resolution of 100 nm has been demonstrated with planar WGs [4], as well as fabrication of two-dimensional WGs providing a point source of $27 \times 44$ nm$^2$ [5]. The incident radiation can be coupled into the guiding layer of x-ray WGs in two different ways: resonant beam coupling (RBC) and front coupling (FC). RBC [6–8] takes place in a three layer WG, with the incident beam at grazing angle transmitted by the very thin upper layer and trapped by the intermediate guiding layer; with this scheme, the incoming beam of several tens of microns can be compressed down to nanometer dimensions and significant effective gain $g$ ($>100$) in flux density can be achieved [9]. In the FC scheme [10], the incoming radiation is directly side coupled with the WG aperture, and the spatial acceptance is therefore equal to the WG gap. However, the angular acceptance is higher than in the RBC mode [11], and prefocusing optics can be efficiently used to obtain a system with a high overall gain $g$ in flux density. Jarre *et al.* have obtained a value of $g \approx 4000$ [5]. Besides the applications which use the waveguide as an optical element capable of providing nanosize beams, other studies rely directly on the interaction of the guided field with a specimen placed inside the WG. This is the case for studies on confined fluids [12] and on thin macromolecular films [13].

In the FC mode, the wave-field propagation can be simply described as a superposition of guided modes, source-free solutions of the Helmholtz equation [10,14]. This description, however, does not take into proper account the interaction of the incoming beam with the cladding material at the entrance of the waveguide. This interaction is described in the following in more detail, both from an analytical point of view and from a computer code based on the numerical solution of parabolic wave equations [15,16]. From this analysis, it appears that several interesting diffraction and refraction phenomena take place, which substantially modify the wave field in the waveguide. The comprehension of these phenomena, besides the fundamental aspect, is of primary importance for production of nanosize beams with predictable features.

We consider a planar hollow x-ray waveguide illuminated on its side at a right angle by a linearly polarized infinite plane wave of wavelength $\lambda = 0.1$ nm and an electric vector parallel to the WG plane. The gap $d$ is limited by two cladding walls (see Fig. 1) with dielectric constant $\varepsilon = (1 - \delta + i\beta)^2$. In the following, silicon is considered as the material constituting the walls. At the photon energies considered in this Letter, $\beta \ll \delta$. Using the paraxial ansatz, the electric field $E$ can be expressed as

$$E_z(x, y) = U(x, y) \exp(ikx), \tag{1}$$

where $U(x, y)$ is the slow changing complex field amplitude and $k = 2\pi/\lambda$ the wave vector. The field is given by the solution of parabolic wave equations (PWEs)

 

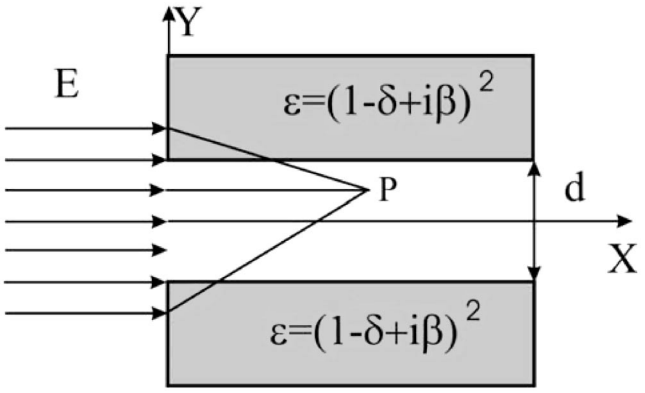


FIG. 1. Geometry of the incoming beam on the side of the waveguide.

$$\begin{aligned} 2ik\partial U/\partial x + \partial^2 U/\partial y^2 = 0, \quad & |y| < d/2, \\ 2ik\partial U/\partial x + \partial^2 U/\partial y^2 + k^2(\varepsilon - 1)U = 0, \quad & |y| > d/2, \end{aligned} \tag{2}$$

with continuity boundary conditions at $y = \pm d/2$.

Kopylov and Popov [17] have shown that the field $U(x, y)$ diffracted by a single dielectric corner (half of the waveguide in our case) can be expressed, in the paraxial approximation, as:

$$\begin{aligned} U(x, y) &= \begin{cases} F(\eta) + \mathrm{M}(\eta, \nu) & \text{vacuum,} \\ (F(\eta) + M(\eta, i\nu))\exp(-\nu^2) & \text{material,} \end{cases} \\ M(x, y) &= (\pi i)^{-1} \int_{-\infty - ia}^{\infty - ia} \exp(-t^2 - 2t\eta\sqrt{i})/\sqrt{t^2 - \nu^2}\, dt \\ &\approx M_1(x, y) + M_2(x, y), \\ \eta &= |y|\sqrt{k/(2x)}, \qquad \nu = \sqrt{kx(\beta + i\delta)}, \qquad k = 2\pi/\lambda, \end{aligned} \tag{3}$$

where $F(x, y)$ is the Fresnel integral and $M(x, y)$ is a new special function whose influence is more significant for weakly absorbing materials. Here, unlike in the WG case, the origin of the $y$ coordinate is taken at the material-vacuum boundary. In the approximation of relatively large distances $x$ from the WG entrance [$x \gg 1/(k\theta_c^2)$, with $\theta_c = (2\delta)^{1/2}$ the critical angle for total reflection], the function $M(x, y)$ can be expressed asymptotically as a sum of two terms

$$M_1(x, y) \approx \sqrt{\frac{2x}{\pi k}} \exp\left(i\frac{ky^2}{2x} - i\frac{\pi}{4}\right) \Big/ \sqrt{\theta_c^2 x^2 - y^2}, \tag{4a}$$

$$M_2(x, y) \approx \sqrt{\frac{2x}{\pi k}} \exp\left(ik\left(\theta_c y - \frac{\theta_c^2}{2}x\right) + i\frac{\pi}{4}\right) \Big/ \sqrt{\theta_c x(\theta_c x - y)}. \tag{4b}$$

The first one $M_1(x, y)$ is a correction to the Fresnel edge diffraction term due to the constituting material of the wall, and the second one $M_2(x, y)$ represents a lateral plane wave propagating in the wall material along the material-vacuum interface $0X$ with enhanced phase velocity $V_p = c/\varepsilon^{1/2}$ and entering into the vacuum at the critical angle $\theta_c$ [17].

The superposition of the direct and diffracted beams with the lateral wave gives rise to an interference pattern of successive maxima and minima [see Fig. 2(a)]. Coordinates of maxima in the spatial intensity distribution can be found from the condition for constructive interference of wave fields described by Eqs. (3) and (4). Figure 2(a) shows the spatial distribution of intensity calculated using the above equations. Figure 2(b) shows the result of a computer simulation based on the PWE numerical solution [15], with the parameters (wavelength, material, and distances) identical to those used in the asymptotic solution. The qualitative agreement is very good.

We extended the same formalism to the analysis of the field at the entrance aperture of the waveguide (see Fig. 1). An approximate solution in the far field zone [$x > (d/2)^2/\lambda$] is the superposition of the field

$$\Phi(x, y) \approx \tilde{\Phi}(k\theta)\exp(-i\pi/4 + ik\theta^2 x/2)/\sqrt{\lambda x}\,, \tag{5a}$$

where

$$\tilde{\Phi}(k\theta) \approx d\left[\frac{\sin(k\theta d/2)}{k\theta d/2} + \frac{\cos(k\theta d/2)}{(kd/2)\sqrt{\theta_c^2 - \theta^2}}\right] \tag{5b}$$

with two lateral plane waves $M_2(x, y)$ [see Eq. (4b)] entering into the vacuum gap from the opposite boundaries $y = \pm d/2$ of the waveguide. In Eq. (5), $\theta = y/x$. The spatial spectral amplitude $\tilde{\Phi}(k\theta)$ in Eqs. (5) includes the sinc function of $(k\theta d/2)$, corresponding to the Fraunhofer diffraction of a plane wave from a thin slit, and a correction term due to the material of the walls. The correction term shifts the positions of the angular spectrum maxima towards smaller angles. It is easy to show that the spectral amplitude $\tilde{\Phi}(k\theta)$ in Eqs. (5) is equal to

$$\tilde{\Phi}(k\theta) \approx \int_{-\infty}^{+\infty} \varphi(y)dy\,, \quad \text{where } \varphi(y) = \begin{cases} \cos(k\theta y) & |y| < d/2, \\ \cos(k\theta d/2)\exp[-k\mu(|y| - d/2)] & \text{else,} \end{cases} \tag{6}$$

where $\mu = (\theta_c^2 - \theta^2)^{1/2}$. For $\theta$ values equal to the waveguide resonance angles $\theta_m$, the function $\varphi(\theta_m) = \varphi_m$ corresponds exactly to the expression of guided modes. Taking the orthogonal modes $\{\varphi_m\}$ of the waveguide as a basis, the

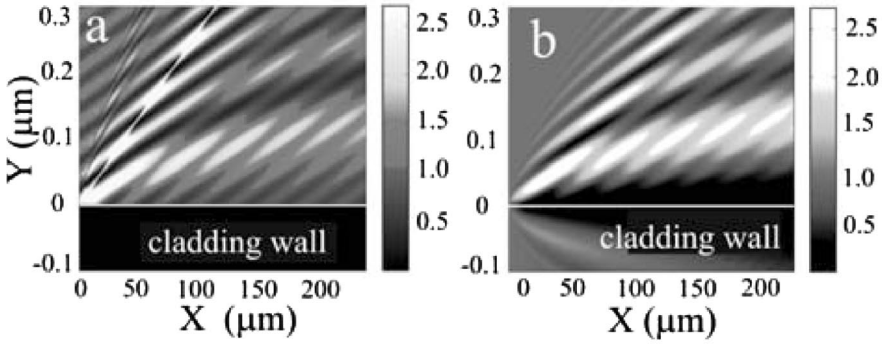


FIG. 2. Diffraction from Si corner: (a) analytical solution; (b) computer simulation. In this case, the origin of the $y$ coordinate is taken at the material-vacuum boundary.

projection of the field $\Phi(x, y)$ on the guided modes at distances $x > x_{\min} = (d/2)^2/\lambda$ is given by [18]

$$\Phi(x, y) = \sum_{m=0}^{m=m_{\max}} c_m(\theta_m)\varphi_m(y), \tag{7}$$

where the coefficients $c_m$ are given by

$$c_m(\theta_m) = \|\varphi_m\|^{-1} \int_{-\infty}^{+\infty} \varphi_m(y)dy \approx \left(\frac{\sin(k\theta_m d/2)}{k\theta_m/2} + \frac{\cos(k\theta_m d/2)}{k\mu_m/2}\right) \Big/ \left(\frac{d}{2} + \frac{\sin(k\theta_m d)}{2k\theta_m} + \frac{\cos^2(k\theta_m d/2)}{k\mu_m}\right). \tag{8}$$

$\theta_m$ are the resonance angles, $\mu_m \approx (\theta_c^2 - \theta_m^2)^{1/2}$, and $m_{\max}$ is the maximum number of allowed resonance modes. Taking into account the propagation factor $\exp(-i\chi_m x)$ for each mode, where in the parabolic approximation, for $\theta \ll \theta_c$, $\chi_m \approx \theta_m^2[k/2 - i(\beta/\delta^{3/2})/(2^{1/2}d)]$ [16], the wave field $\Phi(x, y)$ at any point of the waveguide is given by:

$$\Phi(x, y) = \sum_{m=0}^{m=m_{\max}} c_m(\theta_m)\varphi_m(x)\exp(-i\chi_m x). \tag{9}$$

The total field $U(x, y)$ is therefore given by the superposition of propagating modes Eq. (9) and two laterals waves Eq. (4b) entering into the vacuum gap from the opposite boundaries $y = \pm d/2$ of the waveguide

$$\Psi(x, y) \approx \frac{d}{\sqrt{\lambda x}} \exp(i\pi/4 - ik\theta_c^2 x/2)\frac{\cos(k\theta_c y)}{k\theta_c d/2} \times \exp(ik\theta_c d/2). \tag{10}$$

In Fig. 3, the global intensity distribution in the vacuum guiding layer for a 30 nm gap waveguide with Si walls and photon wavelength $\lambda = 0.1$ nm is shown. The waveguide supports only one mode. Figure 3(a) depicts the asymptotic solution given by Eqs. (9) and (10), and Fig. 3(b) represents the result of the computer simulation based on the numerical solution of the parabolic wave equation [Eq. (2)] [15]. The agreement is very good. Figure 3(c) shows the intensity distribution when the field at the waveguide entrance is a step function [$U(0, y) = 1$ for $y \in [-d/2, d/2]$ and $U(0, y) = 0$ elsewhere], and, therefore, penetration through the cladding walls is excluded. Figure 3 shows that the interference of guided mode with lateral waves introduces strong spatial modulation of the signal.

To the purpose of a more quantitative comparison, Figs. 4(a) and 4(b) show the distribution of the intensity and of the phase of the resulting field along the optical axis $0x$. The dashed line represents the asymptotic solution, the solid line the computer simulation.

The contribution of the field diffracted and refracted by the cladding walls is not only related to the spatial modulation of the signal. Both asymptotic solutions and computer calculations show that the field penetrating into the waveguide from the weakly absorbing cladding walls sig-

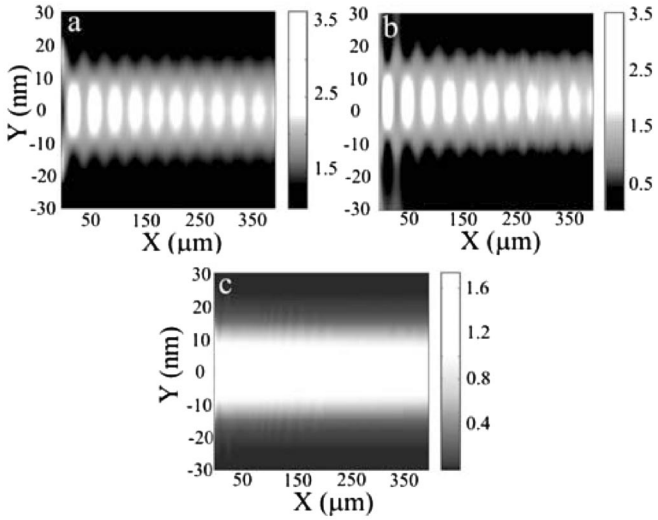


FIG. 3. Total field in a waveguide with Si walls and a 30 nm gap (wavelength = 0.1 nm) with a plane wave at the entrance: (a) asymptotic solution; (b) computer simulation; (c) computer simulation, with a step function field ($U = 1$ in the gap, 0 elsewhere) at the entrance.

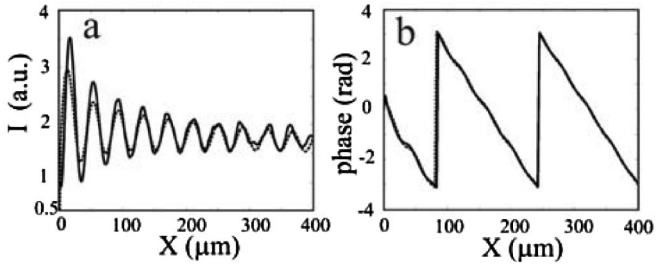


FIG. 4. Variation (a) of the intensity and (b) of the phase along the optical axis $0x$ of a waveguide as the result of the asymptotic solution (dashed line) and computer simulation (solid line).

nificantly increases (approximately 1.5 times) the electromagnetic power in the waveguide compared to the case when the field at the waveguide entrance is a simple step function and therefore penetration through the cladding walls is excluded. In Fig. 5, we report the normalized integrated power within the WG gap as a function of propagation distance $x$.

In conclusion, it has been shown that calculation of the field in a hollow weakly absorbing x-ray waveguide must take into account the interaction of the incoming beam with the cladding material at the entrance of the waveguide. The total field in the guiding vacuum layer can then be expressed as the superposition of guided modes with nonuniform plane waves penetrating into the guiding gap from the cladding walls at the critical angle of reflection $\theta c$ (lateral waves). An asymptotic expression of the total field

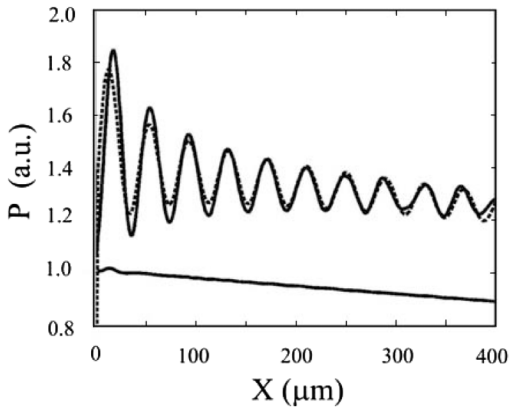


FIG. 5. Normalized value of electromagnetic power integrated within a vacuum gap vs coordinate $x$ calculated for a steplike entrance function (bottom lines) and for a total field calculated following Eqs. (9) and (10) (top lines). The solid lines are the result of computer simulation, and the dashed lines are the result of asymptotic solution.

is given and compared with results of the computer simulation based on numerical solution of the parabolic wave equations. The two independent approaches (asymptotic solution and computer simulation) to the diffraction problem demonstrate very good qualitative and quantitative agreement. In this Letter, we considered as an incident field an infinite plane wave. This is a good approximation as long as the lateral extension of the incident beam is several times the value of the WG gap, which is, in general, limited to a few tens of nanometers. Extension to more complex situations, as, for example, a Gaussian beam with the waist of the same order of magnitude of the gap, is, in principle, possible but outside the scope of this Letter.

The results presented in this Letter demonstrate that it is necessary to include the interaction with cladding layers to obtain an accurate description of the field inside the WG. The capability to predict in the most accurate way the field inside the WG is of relevance for applications, such as microscopy, microdiffraction, etc., which use the nanobeam provided by the WG, and for those applications where the specimen is placed inside the waveguide, as those reported in Refs. [12,13].

The authors gratefully acknowledge partial financial support of Italian projects SPARC and SPARX.

[1] E. Spiller and A. Segmüller, Appl. Phys. Lett. **24**, 60 (1974).
[2] C. Bergemann, H. Keymeulen, and J. F. van der Veen, Phys. Rev. Lett. **91**, 204801 (2003).
[3] F. Pfeiffer *et al.*, Phys. Rev. B **62**, 16 939 (2000).
[4] S. Di Fonzo *et al.*, Nature (London) **403**, 638 (2000).
[5] A. Jarre *et al.*, Phys. Rev. Lett. **94**, 074801 (2005).
[6] Y. P. Feng *et al.*, Appl. Phys. Lett. **67**, 3647 (1995).
[7] S. Lagomarsino *et al.*, J. Appl. Phys. **79**, 4471 (1996).
[8] E. Pfeiffer *et al.*, Science **297**, 230 (2002).
[9] W. Jark *et al.*, Appl. Phys. Lett. **78**, 1192 (2001).
[10] M. J. Zwanenburg *et al.*, Phys. Rev. Lett. **82**, 1696 (1999).
[11] W. Jark and S. Di Fonzo, J. Synchrotron Radiat. **11**, 386 (2004).
[12] M. J. Zwanenburg *et al.*, Phys. Rev. Lett. **85**, 5154 (2000).
[13] T. Salditt *et al.*, Physica (Amsterdam) **336B**, 181 (2003).
[14] J. H. H. Bongaerts *et al.*, J. Synchrotron Radiat. **9**, 383 (2002).
[15] Y. V. Kopylov, A. V. Popov, and A. V. Vinogradov, Opt. Commun. **118**, 619 (1995).
[16] D. Pellicia *et al.* (to be published).
[17] Y. V. Kopylov and A. V. Popov, Radio Sci. **31**, 1815 (1996).
[18] D. Marcuse, *Theory of Dielectric Optical Waveguides* (Academic, New York, 1974).